Int. J. Solids Structures Vol. 26, No. 4, pp. 401–415, 1990
Printed in Great Britain.

0020-7683/90 $3.00+.00

AXISYMMETRIC TRANSIENT ELASTODYNAMIC ANALYSIS BY BOUNDARY ELEMENT METHOD

HUI-CHING WANG and PRASANTA K. BANERJEE
Department of Civil Engineering, State University of New York at Buffalo, 212 Ketter Hall, Buffalo, NY 14260, U.S.A.

(*Received* 11 *April* 1989; *in revised form* 10 *July* 1989)

Abstract—The first formulation of an axisymmetric transient elastodynamic analysis by time domain boundary element method is presented and is implemented in a general purpose system, GPBEST. For the evaluation of boundary convolution integrals, both constant and linear variations in the time domain of displacement and traction fields are given. Transformation of 3-D dynamic kernels into cylindrical coordinates and the integration of kernels along circumferential direction leads directly to an axisymmetric analysis with only 2-D boundary discretization. The numerical integration of these kernels has been done carefully by preserving the causality so that very good accuracy and reliability of the present analysis have been achieved, as can be seen in the examples presented.

INTRODUCTION

For the advantages of the reduction by one dimension of problems and the ease of modelling of unbounded domain, the time-domain boundary element method is gaining more attention in transient dynamic problems of solid mechanics. The time-domain boundary element formulation for the two-dimensional transient dynamic analysis using constant elements has been implemented by Cole *et al.* (1978) for the scalar anti-plane strain problems. Using essentially similar simple implementation, Niwa *et al.* (1980) solved two-dimensional wave scattering problems, Mansur and Brebbia (1982) the two-dimensional transient scalar problem, Mansur and Brebbia (1985) two-dimensional transient elastodynamic problems, Rice and Sadd (1984) the anti-plane strain wave scattering problem, Spyrakos and Beskos (1986) the transient dynamic response of rigid strip foundation, and Antes and von Estorff (1986) used it for dynamic solid–fluid interaction analysis. All of these implementations were rather crude and did not give results with sufficient accuracy. This situation has been improved significantly by Israil and Banerjee (1989) in which they introduce higher-order shape functions in space and time for the first time in a two-dimensional analysis.

Compared to two-dimensional problems, three-dimensional transient dynamic analysis needs more computing efforts and much more sophisticated numerical implementation, and consequently was not attempted until Karabalis and Beskos (1984) developed a simplified formulation for the special case of rigid surface foundations. The first general three-dimensional time-domain direct boundary element formulation for transient dynamic analysis was given by Banerjee and Ahmad (1985) and Banerjee *et al.* (1986) using a constant temporal and quadratic spatial interpolation function for the field variables. A linear temporal variation was lately published by Ahmad and Banerjee (1988) for the general three-dimensional transient elastodynamic analysis and was combined with the use of domain integral by Ahmad (1986) for the inelastic transient analysis of a circular bar under a step end load.

To the best of the authors' knowledge, the numerical implementation of BEM for the time domain axisymmetric transient dynamic analysis has not appeared in the published literature. In this paper, the first numerical implementation for an axisymmetric transient elastodynamic analysis by using the general three-dimensional formulation suggested by Banerjee and Ahmad (1985) is proposed. The results of the analysis for a number of axisymmetric problems have been verified by comparing with known analytical solutions.

TIME DOMAIN BEM FORMULATION

The governing equation for the dynamic small-displacement field $u_i(x, t)$ in an isotropic homogeneous elastic body can be derived by considering the equations of equilibrium, the

constitutive law and the kinematic equations as

$$(c_1^2-c_2^2)u_{j,ij}(x,t)+c_2^2u_{i,jj}(x,t)+b_i(x,t)-\frac{\partial^2u_i(x,t)}{\partial t^2}=0 \tag{1}$$

where $b_i(x,t)$ is the body force, and c_1 and c_2 are the propagation velocities of the pressure wave and shear wave, respectively, and are given as

$$c_1=\left(\frac{\lambda+2\mu}{\rho}\right)^{1/2} \tag{2a}$$

$$c_2=\left(\frac{\mu}{\rho}\right)^{1/2} \tag{2b}$$

in which λ and μ are Lamé constants and ρ is the mass density. At time t, considering a domain V bounded by surface S, the displacement at point ξ can be obtained via the reciprocal work theorem in an integral form as

$$\begin{aligned}c_{ij}u_i(\xi,t)=&\int_S\int_0^t[G_{ij}(x,\tau;\xi,t)t_i(x,\tau)-F_{ij}(x,\tau;\xi,t)u_i(x,\tau)]\,\mathrm{d}\tau\,\mathrm{d}S(x)\\&+\rho\int_V\int_0^t G_{ij}(x,\tau;\xi,t)b_i(x)\,\mathrm{d}\tau\,\mathrm{d}V(x)\\&+\rho\int_V\left[\frac{\partial u_i(x,0)}{\partial t}G_{ij}(x,t;\xi,0)+u_i(x,0)\frac{\partial G_{ij}(x,t;\xi,0)}{\partial t}\right]\mathrm{d}V(x)\end{aligned} \tag{3}$$

where c_{ij} is a constant, $G_{ij}(x,\tau;\xi,t)$ and $F_{ij}(x,\tau;\xi,t)$ are the fundamental solutions (Appendix A) which can be found in Eringen and Suhubi (1975). For a point ξ within V, c_{ij} is δ_{ij}, for ξ on a smooth boundary S, $c_{ij}=\delta_{ij}/2$, and $c_{ij}=0$ elsewhere. If the body force is absent and the domain is initially at rest, then only the surface integrals remain, i.e.

$$c_{ij}u_i(\xi,t)=\int_S\int_0^t[G_{ij}(x,\tau;\xi,t)t_i(x,\tau)-F_{ij}(x,\tau;\xi,t)u_i(x,\tau)]\,\mathrm{d}\tau\,\mathrm{d}S(x). \tag{4}$$

For axisymmetric problems, the field variables are independent of circumferential angle, so the equation is expressed in cylindrical coordinates (r,θ,z) as

$$c_{ij}u_i'(\xi,t)=2\int_L\int_0^\pi\int_0^t[G_{ij}'(x,\tau;\xi,t)t_i'(x,\tau)-F_{ij}'(x,\tau;\xi,t)u_i'(x,\tau)]\,\mathrm{d}\tau\,\mathrm{d}\theta_x\,r_x\,\mathrm{d}L(x) \tag{5}$$

where L is the generator of axisymmetric body and

$$u_i'(x,t)=\begin{Bmatrix}u_r(x,t)\\u_z(x,t)\end{Bmatrix}\quad t_i'(x,t)=\begin{Bmatrix}t_r(x,t)\\t_z(x,t)\end{Bmatrix}$$

$$G_{ij}'(x,\tau;\xi,t)=\begin{bmatrix}G_{rr}&G_{rz}\\G_{zr}&G_{zz}\end{bmatrix}=\begin{bmatrix}G_{11}\cos\theta_x+G_{21}\sin\theta_x & G_{13}\cos\theta_x+G_{23}\sin\theta_x\\G_{31}&G_{33}\end{bmatrix}$$

$$F_{ij}'(x,\tau;\xi,t)=\begin{bmatrix}F_{rr}&F_{rz}\\F_{zr}&F_{zz}\end{bmatrix}=\begin{bmatrix}F_{11}\cos\theta_x+F_{21}\sin\theta_x & F_{13}\cos\theta_x+F_{23}\sin\theta_x\\F_{31}&F_{33}\end{bmatrix}.$$

Note that the factor 2 in eqn (5) is due to the symmetry of kernels G and F with respect to the axis $\theta=0$. The θ component displacement is not seen here because it is independent of

other components for axisymmetric problems and a direct integration with respect to θ must be carried out. Unfortunately it is not possible to do this analytically because of the discontinuous nature of the kernel functions (Appendix A) and therefore a suitable numerical integration scheme as discussed later is needed.

Time marching scheme

Considering an N-step time discretization $t = N\Delta t$ and a discretization of generator $L = \Sigma_{m=1}^{M} L_m$, we can rewrite eqn (5) as

$$c_{ij}u_i'(\xi, N\Delta t) = 2\sum_{m=1}^{M}\int_{L_m}\int_0^{\pi}\sum_{n=1}^{N}\int_{(n-1)\Delta t}^{n\Delta t} G_{ij}'(x,\tau;\xi,n\Delta t)t_i'(x,\tau)\,\mathrm{d}\tau\,\mathrm{d}\theta_x\, r_x\,\mathrm{d}L_m(x)$$
$$-2\sum_{m=1}^{M}\int_{L_m}\int_0^{\pi}\sum_{n=1}^{N}\int_{(n-1)\Delta t}^{n\Delta t} F_{ij}'(x,\tau;\xi,n\Delta t)u_i'(x,\tau)\,\mathrm{d}\tau\,\mathrm{d}\theta_x\, r_x\,\mathrm{d}L_m(x). \quad (6)$$

So far, this equation still remains an exact solution because no approximation has been made. Then the approximations of boundary displacements and tractions in the time interval $[(n-1)\Delta t, n\Delta t]$ are made as

$$u_i(x,\tau) = M_1 u_i(x,(n-1)\Delta t) + M_2 u_i(x, n\Delta t) \quad (7a)$$

$$t_i(x,\tau) = M_1 t_i(x,(n-1)\Delta t) + M_2 t_i(x, n\Delta t) \quad (7b)$$

and the quadratic approximations on the discrete element L_m are made as

$$u_i(x,t) = N^k(x)u_i(x^k,t) = N^1 u_i(x^1,t) + N^2 u_i(x^2,t) + N^3 u_i(x^3,t) \quad (7c)$$

$$t_i(x,t) = N^k(x)t_i(x^k,t) = N^1 t_i(x^1,t) + N^2 t_i(x^2,t) + N^3 t_i(x^3,t) \quad (7d)$$

where M_1 and M_2 are the approximation function in time domain, $N^k(x)$ is an interpolation function, and x^k is the kth collocation boundary point on L_m. For a constant time approximation, M_1 vanishes and M_2 is 1, or $M_1 = M_2 = 0.5$ for a constant averaging approximation. If a linear time variation is used, we have for $t_a < \tau \leqslant t_b$

$$M_1(\tau) = \frac{t_b - \tau}{t_b - t_a} \quad (8a)$$

$$M_2(\tau) = 1 - \frac{t_b - \tau}{t_b - t_a}. \quad (8b)$$

For isoparametric elements, interpolation functions are chosen to be the same as the shape functions used in the mapping of boundary elements. For a quadratic element, these interpolation functions or shape functions can be found in Banerjee and Butterfield (1981). Thus equation (6) can be rewritten in the form

$$c_{ij}u_i'(\xi,N\Delta t) - 2\sum_{m=1}^{M}\int_{L_m}\int_0^{\pi}\int_{(N-1)\Delta t}^{N\Delta t} G_{ij}'(x,\tau;\xi,N\Delta t)M_2\,\mathrm{d}\tau\,\mathrm{d}\theta_x\, N^k(x)r_x\,\mathrm{d}L_m(x)t_i(x^k,N\Delta t)$$
$$+2\sum_{m=1}^{M}\int_{L_m}\int_0^{\pi}\int_{(N-1)\Delta t}^{N\Delta t} F_{ij}'(x,\tau;\xi,N\Delta t)M_2\,\mathrm{d}\tau\,\mathrm{d}\theta_x\, N^k(x)r_x\,\mathrm{d}L_m(x)u_i(x^k,N\Delta t)$$
$$= 2\sum_{m=1}^{M}\int_{L_m}\int_0^{\pi}\int_{(N-1)\Delta t}^{N\Delta t} G_{ij}'(x,\tau;\xi,N\Delta t)M_1\,\mathrm{d}\tau\,\mathrm{d}\theta_x\, N^k(x)r_x\,\mathrm{d}L_m(x)t_i(x^k,(N-1)\Delta t)$$
$$-2\sum_{m=1}^{M}\int_{L_m}\int_0^{\pi}\int_{(N-1)\Delta t}^{N\Delta t} F_{ij}'(x,\tau;\xi,N\Delta t)M_1\,\mathrm{d}\tau\,\mathrm{d}\theta_x\, N^k(x)r_x\,\mathrm{d}L_m(x)u_i(x^k,(N-1)\Delta t)$$

$$+2\sum_{m=1}^{M}\sum_{n=1}^{N-1}\int_{L_m}\int_0^{\pi}\int_{(N-1)\Delta t}^{N\Delta t} G'_{ij}(x,\tau;\xi,N\Delta t)M_2\,\mathrm{d}\tau\,\mathrm{d}\theta_x\,N^k(x)r_x\,\mathrm{d}L_m(x)t_i(x_k,n\Delta t)$$

$$-2\sum_{m=1}^{M}\sum_{n=1}^{N-1}\int_{L_m}\int_0^{\pi}\int_{(N-1)\Delta t}^{N\Delta t} F'_{ij}(x,\tau;\xi,N\Delta t)M_2\,\mathrm{d}\tau\,\mathrm{d}\theta_x\,N^k(x)r_x\,\mathrm{d}L_m(x)u_i(x^k,n\Delta t)$$

$$+2\sum_{m=1}^{M}\sum_{n=1}^{N-1}\int_{L_m}\int_0^{\pi}\int_{(N-1)\Delta t}^{N\Delta t} G'_{ij}(x,\tau;\xi,N\Delta t)M_1\,\mathrm{d}\tau\,\mathrm{d}\theta_x\,N^k(x)r_x\,\mathrm{d}L_m(x)t_i(x^k,(n-1)\Delta t)$$

$$-2\sum_{m=1}^{M}\sum_{n=1}^{N-1}\int_{L_m}\int_0^{\pi}\int_{(N-1)\Delta t}^{N\Delta t} F'_{ij}(x,\tau;\xi,N\Delta t)M_1\,\mathrm{d}\tau\,\mathrm{d}\theta_x\,N^k(x)r_x\,\mathrm{d}L_m(x)u_i(x^k,(n-1)\Delta t). \tag{9}$$

Choosing q collocating points on the generator L and letting ξ approach these collocating points, and noting the fact that

$$\int_{t_a}^{t_b} G'_{ij}(x,\tau;\xi,N\Delta t)f(t_b-\tau)\,\mathrm{d}\tau = \int_0^{t_b-t_a} G'_{ij}(x,\tau;\xi,N\Delta t-t_a)f(t_b-t_a-\tau)\,\mathrm{d}\tau \tag{10a}$$

$$\int_{t_a}^{t_b} F'_{ij}(x,\tau;\xi,N\Delta t)f(t_b-\tau)\,\mathrm{d}\tau = \int_0^{t_b-t_a} F'_{ij}(x,\tau;\xi,N\Delta t-t_a)f(t_b-t_a-\tau)\,\mathrm{d}\tau \tag{10b}$$

we are able to form a set of equations in the following matrix form (Ahmad and Banerjee, 1988):

$$\begin{aligned}-[G_2^1]\{t(x^k,N\Delta t)\}+[F_2^1]\{u(x^k,N\Delta t)\} &= [G_1^1]\{t(x^k,(N-1)\Delta t)\}-[F_1^1]\{u(x^k,(N-1)\Delta t)\}\\ &+\sum_{n=1}^{N-1}\{[G_2^{N-n+1}]\{t(x^k,n\Delta t)\}-[F_2^{N-n+1}]\{u(x^k,n\Delta t)\}\\ &+[G_1^{N-n+1}]\{t(x^k,(n-1)\Delta t)\}-[F_1^{N-n+1}]\{u(x^k,(n-1)\Delta t)\}\}.\end{aligned} \tag{11}$$

Note that during every time step, only four more matrices have to be formed until the largest distance between any two different points in the domain is smaller than the distance travelled by the shear wave at which time all the new matrices will be null matrices (see Appendix B). The coefficients in these matrices represent the effect on the current status due to the dynamic history of displacements and the tractions in the domain at previous times. After a certain time step all these effects have been included in the calculated matrices if a bounded domain is considered and no further integration is necessary. After applying boundary conditions and initial conditions, we get a system equation at the Nth time step for the transient analysis as

$$\begin{aligned}[A_2^1]\{X^N\} &= [B_2^1]\{Y^N\}-[A_1^1]\{X^{N-1}\}+[B_1^1]\{Y^{N-1}\}\\ &+\sum_{n=1}^{N-1}(-[A_2^{N-n+1}]\{X^n\}+[B_2^{N-n+1}]\{Y^n\}-[A_1^{N-n+1}]\{X^{n-1}\}+[B_1^{N-n+1}]\{Y^{n-1}\})\end{aligned} \tag{12}$$

where X^i denotes the unknown field variables and Y^i the known boundary conditions at time $t = i\Delta t$.

NUMERICAL TREATMENTS

As seen in equation (6), the boundary discretization is needed only for the generator of axisymmetric body just like any ordinary axisymmetric boundary element analyses. But three levels of integrals of kernels have to be computed. First, the convolution integrals with respect to time are evaluated according to the analytical procedure proposed by Ahmad and Banerjee (1988), as shown in Appendix B.

Second, the integrals along the circumferential direction cannot be evaluated analytically and therefore a numerical integration scheme must be used. This must be done with sufficient care because each of the kernels G and F consists of two components, a pressure wave propagation and a shear wave propagation, and as a result both kernels are not continuous. Moreover, at the first (or the leading) time step, the kernel F is strongly singular and the kernel G is weakly singular, which makes the application of ordinary Gaussian quadrature difficult, especially in the integration of kernel F. As for the remaining time steps, they are not singular and the integration is simpler provided one allows for the discontinuous nature of these functions. At the first time step, kernel F is broken into two parts,

$$(F'_{ij})_{\text{trans}} = (F'_{ij})_{\text{static}} + [(F'_{ij})_{\text{trans.}} - (F'_{ij})_{\text{static}}].$$

The first part is identical to the kernel for elastostatics and contains the same strong singularity. The integration of the static kernel with respect to θ can be done analytically, as was shown by Rizzo and Shippy (1979) and Mayr *et al.* (1980). The second part is no longer strongly singular and therefore can be integrated numerically. The integration of G is also carried out in the same way for the convenience of programming, although its singularity is weaker. Since the transient kernels are not continuous functions, the interval $[0, \pi]$ during $[(n-1)\Delta t, n\Delta t]$ is divided into five segments for the first time step integration

Segment a: $r(x, \xi) \leqslant c_2(n-1)\Delta t$

Segment b: $c_2(n-1)\Delta t < r(x, \xi) \leqslant$ smaller of $[c_2 n\Delta t, c_1(n-1)\Delta t]$

Segment c: smaller of $[c_2 n\Delta t, c_1(n-1)\Delta t] < r(x, \xi) \leqslant$ greater of $[c_2 n\Delta t, c_1(n-1)\Delta t]$

Segment d: greater of $[c_2 n\Delta t, c_1(n-1)\Delta t] < r(x, \xi) \leqslant c_2(n-1)\Delta t$

Segment e: $r(x, \xi) \leqslant c_2(n-1)\Delta t$

where $r(x, \xi)$ is the distance between points (r_x, θ_x, z_x) and $(r_\xi, 0, z_\xi)$. Thus in each segment, the integrated functions are made continuous and therefore better accuracy can be obtained this way compared to a uniform segmentation or no segmentation with a number of integrating points. Although transient kernels vanish in segments a and e, the integrations on two segments are still needed for static kernels. The number of these segments depends on the magnitude of the time step and the distance between point ξ and the integrated ring $x(r_x, \theta_x, z_x)$ within the $\theta_x = 0, \pi$ interval. Because the coefficients of matrices $[G]$ and $[F]$ found at the first time step are needed as leading matrices in each time step, very high accuracy in the integration must be achieved to prevent build-up of errors. For this reason, up to 10 Gaussian points in each segment are used; moreover further segmentations are needed if the point ξ is close to the integrated ring. Although the cost of this integration is high, it is only a small part of the time stepping analysis because it is needed only at the first time step and the coefficients are reusable in other time steps.

For the remaining time steps, the kernels are regular and well behaved, so the entire set of transient dynamic kernels can be numerically integrated in the circumferential direction. Since the integrals of kernels G and F vanish in segments a and e, only the numerical integrations in three segments b, c and d are needed. In each segment, only three Gaussian points are used and total number of segments is no more than three, even when point x is close to the integrated ring.

Finally, integration on the discrete elements of generator L must be carried out. At the first time step, 10 segments are used and the number of Gaussian points in each segment depends on the distance between the point ξ and the integrated discrete element L_m. For the remaining time steps, the exact interval where the integration is needed can be found by examining the behavior of kernels; as a result, less computing effort during one time step is needed compared to that at the first time step. Since the static G and F matrices are automatically available during the calculation at the leading time step, the diagonal blocks of F for the leading time step can be found by using the elastic solutions for the inflation

and rigid body displacements for the static part (Nigam, 1980) and adding to them the integrated result of the difference between the static and dynamic kernels in the usual manner (Banerjee and Ahmad, 1985).

The analysis outlined above has been implemented in a general purpose analysis system GPBEST and therefore automatically inherits its large infrastructural facilities such as multiple regions, local boundary conditions, sliding interfaces, etc. The examples presented below have been specially designed to demonstrate the accuracy and usefulness of this implementation. Detailed engineering applications to more complex problems involving multizone materials, sliding interfaces, etc. will be developed in a later paper.

NUMERICAL EXAMPLES

(1) *Radial expansion of a spherical cavity in an infinite domain*

Consider a spherical cavity (radius a) in an infinite medium (Poisson ratio $v = 0.25$) under a suddenly applied internal pressure $P_0H(t)$. The analytical solution for displacement can be found in the book by Timoshenko and Goodier (1979). This problem is analyzed using the present analysis with an eight quadratic boundary element mesh (Fig. 1) and a time step of $\Delta t = 0.1715\, a/c_1$. The displacement and the tangential stress at the cavity surfaced are plotted in Figs 2 and 3 and are compared with the theoretical solutions. Excellent results are obtained by using such a simple mesh. Note the theoretical tangential stress jumps to $-2/3$ just after the internal pressure is applied, i.e. $t = 0^+$. To get this compressive stress value, a smaller time step of $\Delta t' = 0.25\Delta t$ is used for a three time step analysis, the results of which are also shown in Fig. 3. The tangential stresses for the remaining time steps are obtained by using the larger time step. Both the displacement and the stress approach the corresponding elastostatic solutions as time increases.

(2) *A point load on a half space*

The second example for verification is a half space under a suddenly applied point load. The analytical formulation of this problem was first given by Lord Rayleigh (1885). Pekeris (1955) gave the theoretical solution for the axisymmetric case and the result for Poisson ratio $v = 0.25$. The problem is again solved by the present analysis. A parabolic distribution of circular load on a disk of radius = a (Fig. 4) is specified as the only applied loading instead of a concentrated point force. For a point far away such an applied loading is going to behave like a concentrated point force. A time step $\Delta t = 0.1\, a/c_2$ is chosen. Two discretizations are used of which mesh 1 has 30 elements including four elements on the disk with a typical element length on the stress-free surface of $10c_2\Delta t$ and mesh 2 has 61 elements including eight elements on the disk with a typical element length on the free

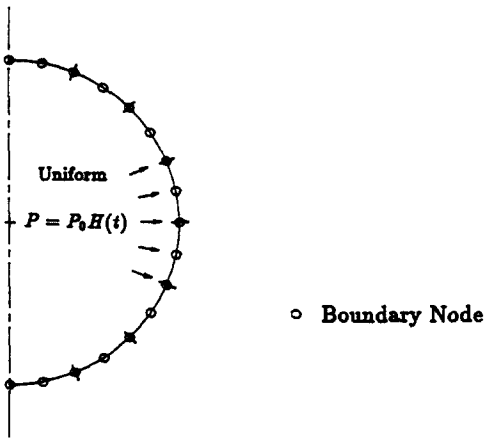

Fig. 1. Boundary discretization of a spherical cavity (radius a).

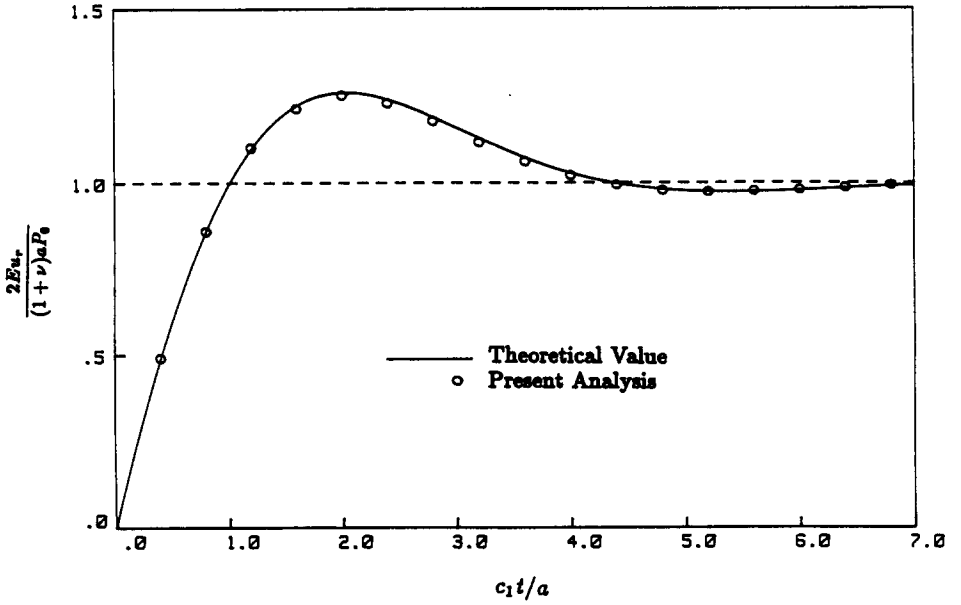

Fig. 2. Radial displacement at the surface of spherical cavity under uniform internal pressure $P_0H(t)$.

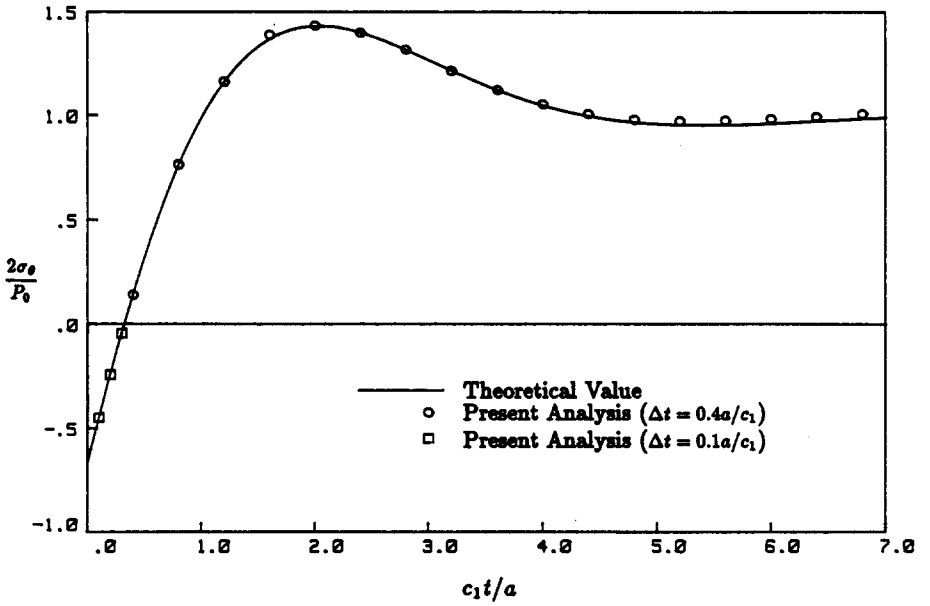

Fig. 3. Tangential stress at the surface of spherical cavity under uniform internal pressure $P_0H(t)$.

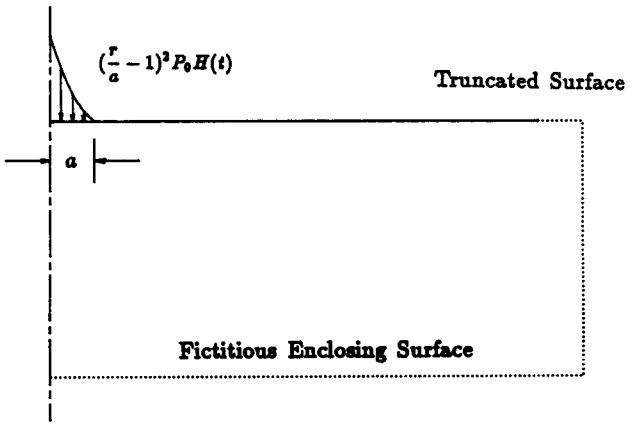

Fig. 4. A half space under surface loading $P_0(r/a-1)^2H(t)$ and its boundary approximation.

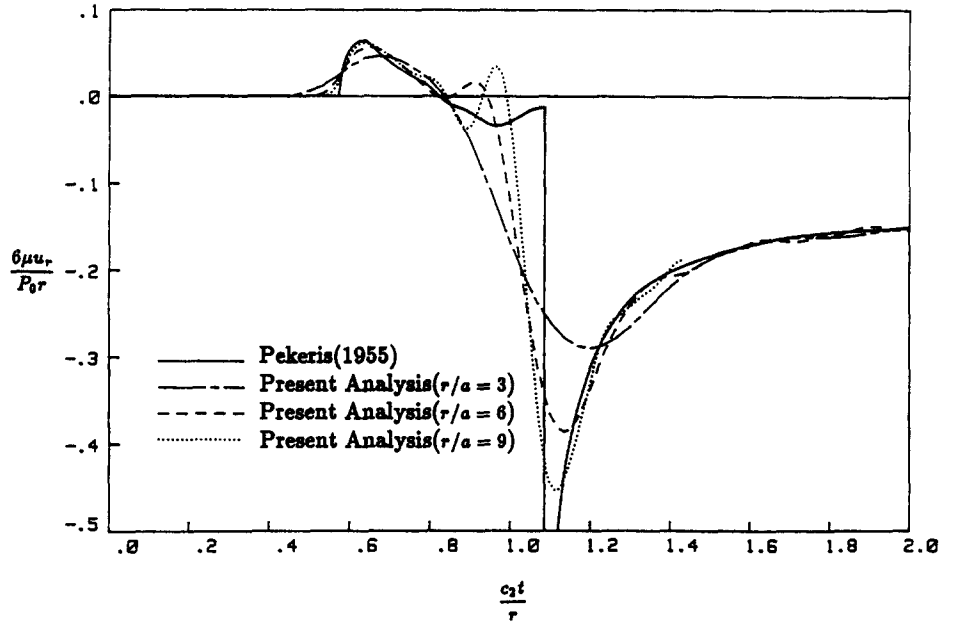

Fig. 5. Radial displacement at the surface of a half space by mesh 1 ($\Delta t = 0.1a/c_2$).

surface of $3c_2\Delta t$. Henry and Banerjee (1988) found that a fictitious enclosing surface is needed for a truncated boundary discretization to obtain the correct diagonal coefficients of the F matrix in axisymmetric elastostatic and elastoplastic analyses. It is also needed in the present transient analysis because of the use of static kernels in evaluating coefficients at the first time step. On these enclosing surface elements, only the integration of static kernels is needed so that the correct diagonal coefficients of the dynamic F matrix could be evaluated. The results of the analysis are plotted in Figs 5–8. As expected, when the observation point is further away from the loaded disk, both the radial and vertical displacement histories are closer to the theoretical solutions. The finer mesh (mesh 2), as expected, gives better results than the coarser one (mesh 1). The analysis correctly repro-

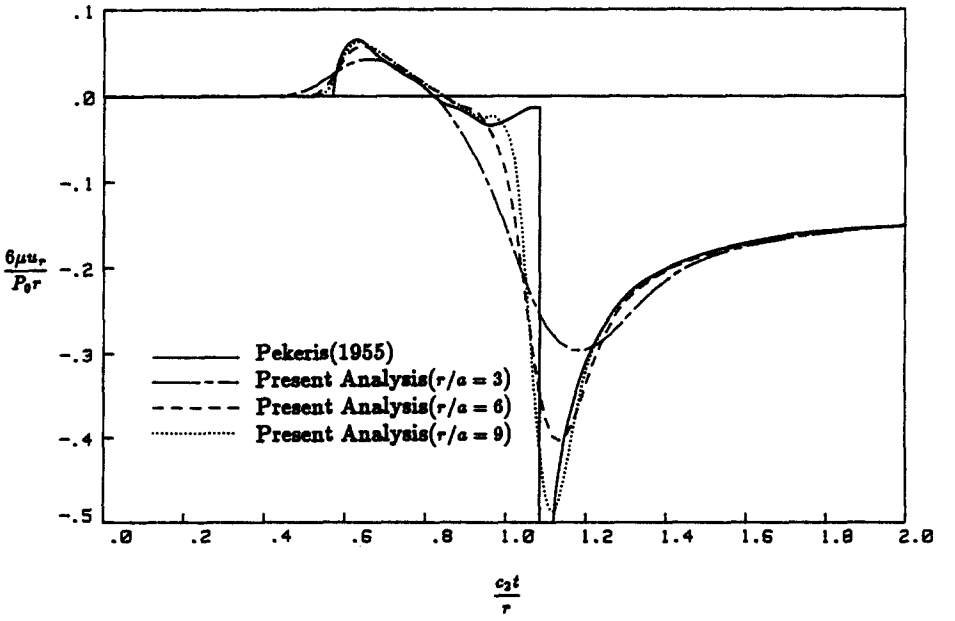

Fig. 6. Radial displacement at the surface of a half space by mesh 2 ($\Delta t = 0.1a/c_2$).

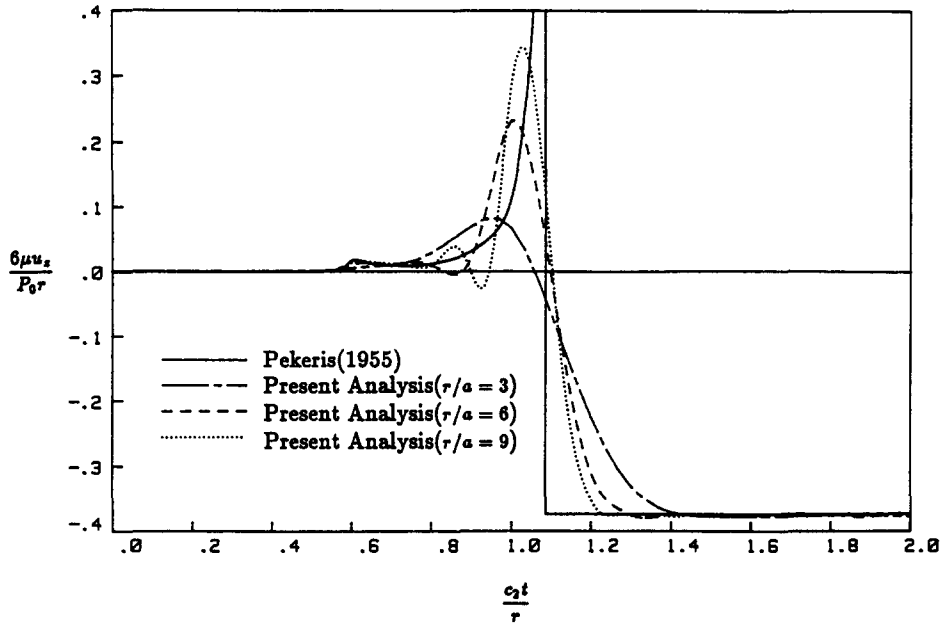

Fig. 7. Vertical displacement at the surface of a half space by mesh 1 ($\Delta t = 0.1a/c_2$).

duces the arrival of Rayleigh waves although it is not implicitly present in the kernel functions G and F.

(3) *A circular notched bar under a compressive impulse*

A circular notched bar (Fig. 9) supported by rollers at one end is subjected to a sudden compressive loading at its free end. The Poisson ratio is 0.25 again. The elastic modulus E, density ρ and the applied sudden load $P_0H(t)$ are given in consistent units as

$$E = 12000 \quad \rho = 1.0 \quad P_0 = 0.5.$$

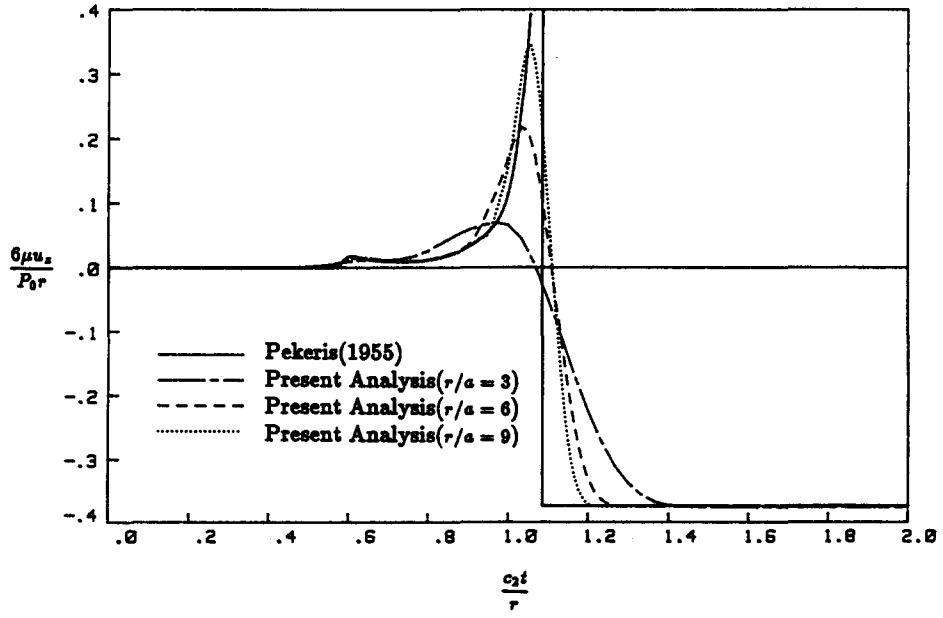

Fig. 8. Vertical displacement at the surface of a half space by mesh 2 ($\Delta t = 0.1a/c_2$).

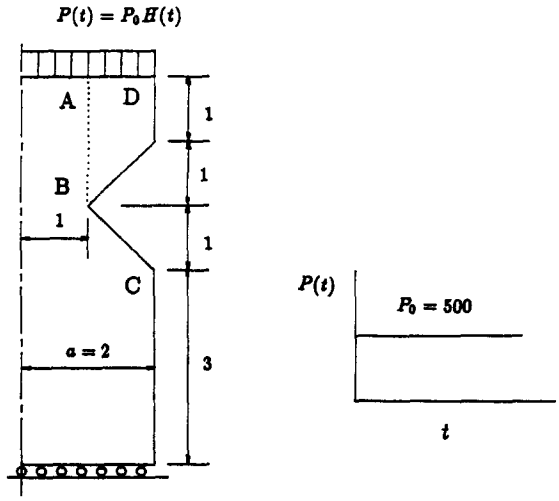

Fig. 9. A notched circular bar supported at one end and subjected to vertical loading $P_0H(t)$ at the other end.

The displacement histories of the observation point at the edge of the notch are plotted in Fig. 10 which are obtained by the present analysis with two different meshes (Figs 11 and 12). Figure 11 shows the one-region mesh having 22 elements and Fig. 12 the two-region mesh having a total of 28 elements. In Fig. 10, it can be seen that the displacement histories by two discretization are the same except that a small upward displacement (amplified in Fig. 13) is found for the one-region discretization before the theoretical arrival time of a pressure wave. The theoretical arrival time of the wavefront should be the time for a wave travelling along the path ABC (Fig. 9) instead of the direct straight path DC. Before theoretical arrival time, the displacement at point C should be zero. Antes and von Estorff (1987) found a magnified version of such a problem in a two-dimensional analysis of half space problems with a notch using constant boundary elements with a linear

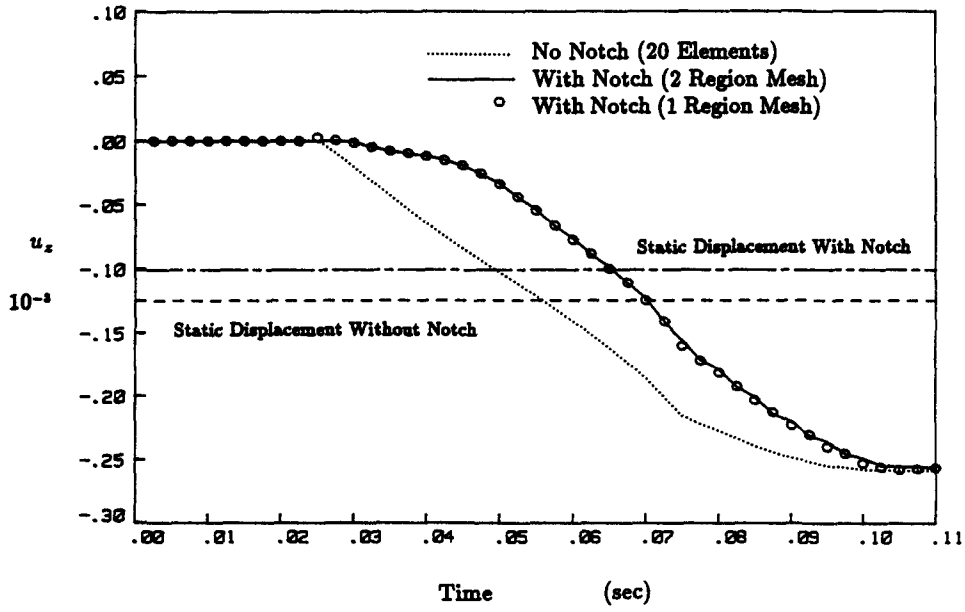

Fig. 10. Vertical displacement at the edge of the notch (point C in Fig. 4).

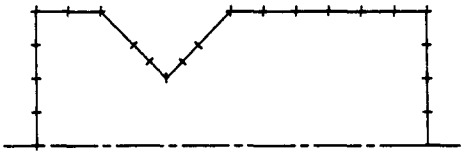

Fig. 11. One-region discretization (22 elements) of a notched bar.

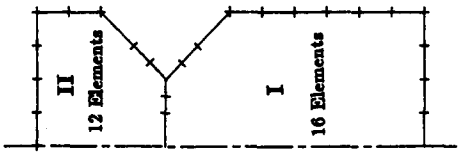

Fig. 12. Two-region discretization of a notched bar.

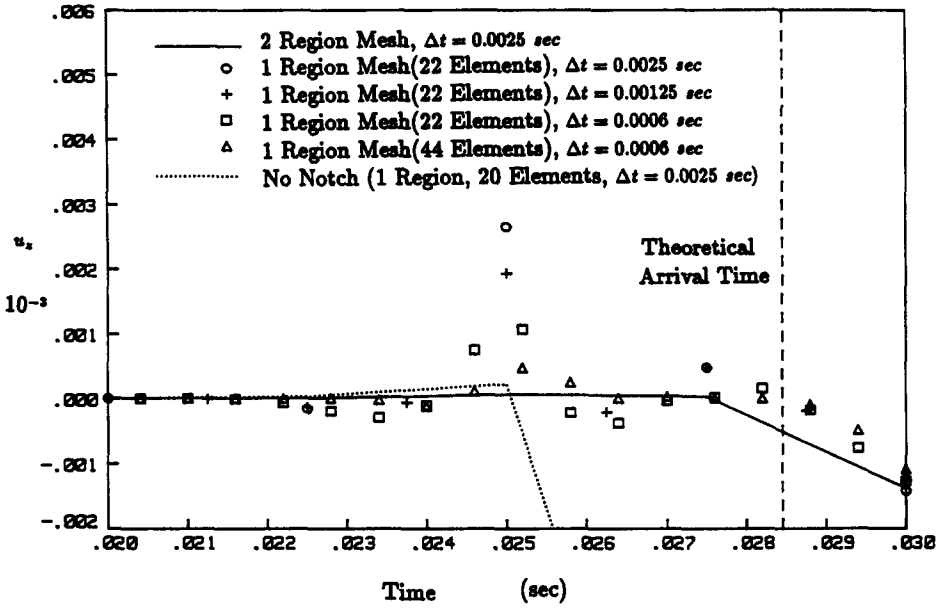

Fig. 13. Convergence in the arrival time of wavefront at point C.

time variation. They suggested that to correct this error convex subregions should be used. But in many cases, it is impossible to do so. In fact, this small error is a numerical error due to the size of the time step and the approximations of the displacement field, especially around the notch. Since the calculations of the coefficient matrices are never exact, there is some false effect before the real wave arrives. If the adopted time steps are correct and the discretization is sufficiently fine then such an error would vanish. To explore this, two smaller time steps and a finer mesh were used for a more detailed analysis. In Fig. 13, focusing on this small error, we can see that as smaller time steps are used, this error reduces. Note that the element length has to be compatible with the distance travelled by the waves in a given time step for accurate integration and a good representation of displacement and traction fields by using shape functions. The time step should be small enough to keep the variations of displacement and traction fields linear in time. Of course, a better way of avoiding this difficulty is to use a multiregion discretization or keep all the regions convex whenever such a discretization is possible. Moreover, a multiregion

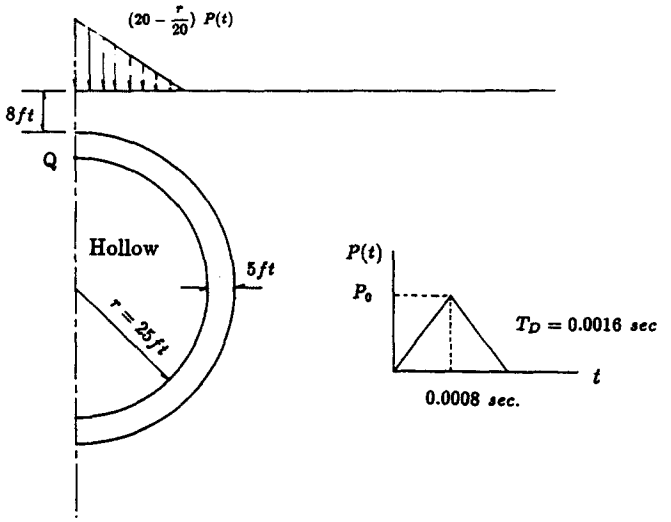

Fig. 14. An underground spherical shell under a blast load on the ground surface.

discretization not only saves computing time, especially for long and slender domains, but also improves the stability of the system. It can be seen that one-region results are never as good as two-region results (Fig. 13).

(4) *An underground spherical shell subject to a blasting on ground*

An underground spherical concrete shell structure is shown in Fig. 14 and is subjected to a triangular blast loading on the ground surface immediately above. The material properties of soil and reinforced concrete are given as

$$E_{\text{soil}} = 4.5\times 10^6 \text{ psf} \quad \nu_{\text{soil}} = 1/3 \quad \rho_{\text{soil}} = 3.23 \text{ lb}\cdot\text{s}^2\,\text{ft}^{-4}$$
$$E_{\text{conc}} = 4.5\times 10^8 \text{ psf} \quad \nu_{\text{conc}} = 0.15 \quad \rho_{\text{conc}} = 4.66 \text{ lb}\cdot\text{s}^2\,\text{ft}^{-4}.$$

The blast load is modelled as $(20-r/20)P(t)$ for $r \leqslant 20$ ft where $P(t)$ is a triangular pulse function (Fig. 14). To analyze the time-dependent response of a shell structure, a two-region mesh as shown in Fig. 15 was used. Since the velocity of wave propagation in

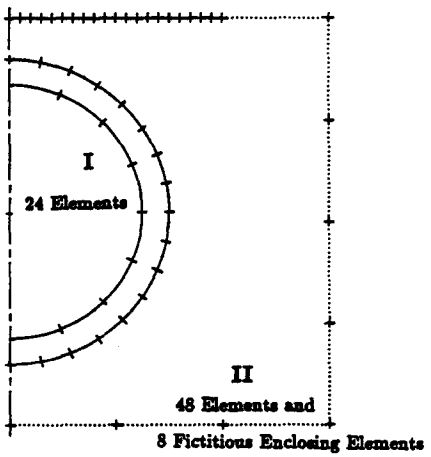

Fig. 15. Two-region boundary discretization for an underground spherical shell.

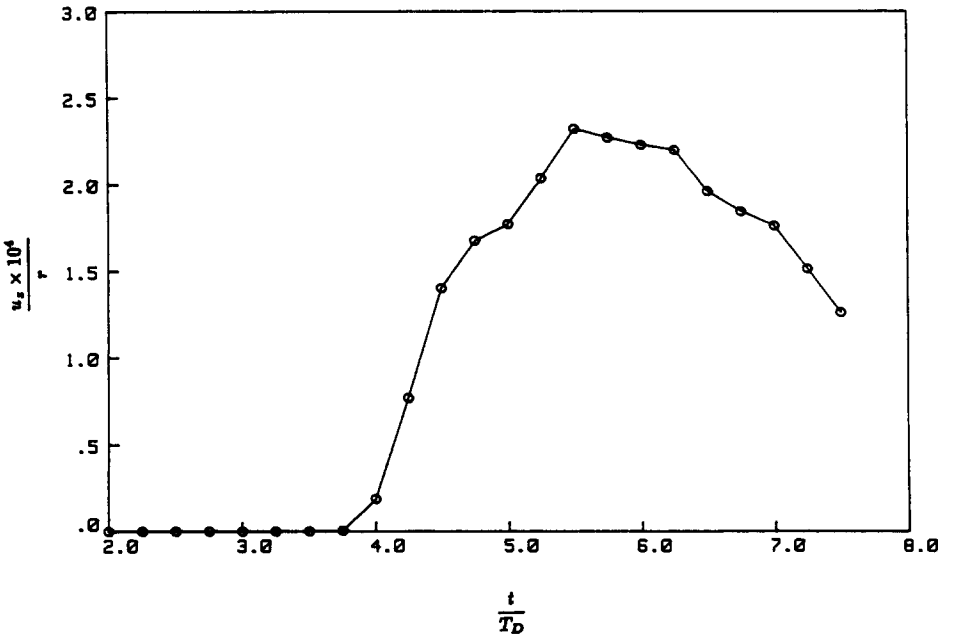

Fig. 16. Vertical displacement at the top (point Q in Fig. 14) of the internal wall of an underground spherical shell.

concrete is faster than that in soil, a coarser discretization can be used for the concrete shell structure. Note that the ground surface is truncated at the distance that the wave had not reached during the time of interest, so the mesh is a very simple one. If a longer response is warranted, a truncated boundary well away from the shell may be needed. For the same reason described in the second example, a fictitious enclosing surface having 10 enclosing elements was used. The vertical displacement and tangential stress histories at point Q (see Fig. 14) are plotted in Figs 16 and 17, respectively. The maximum tangential stress is about $1.03P_0$ where P_0 is the maximum of $P(t)$.

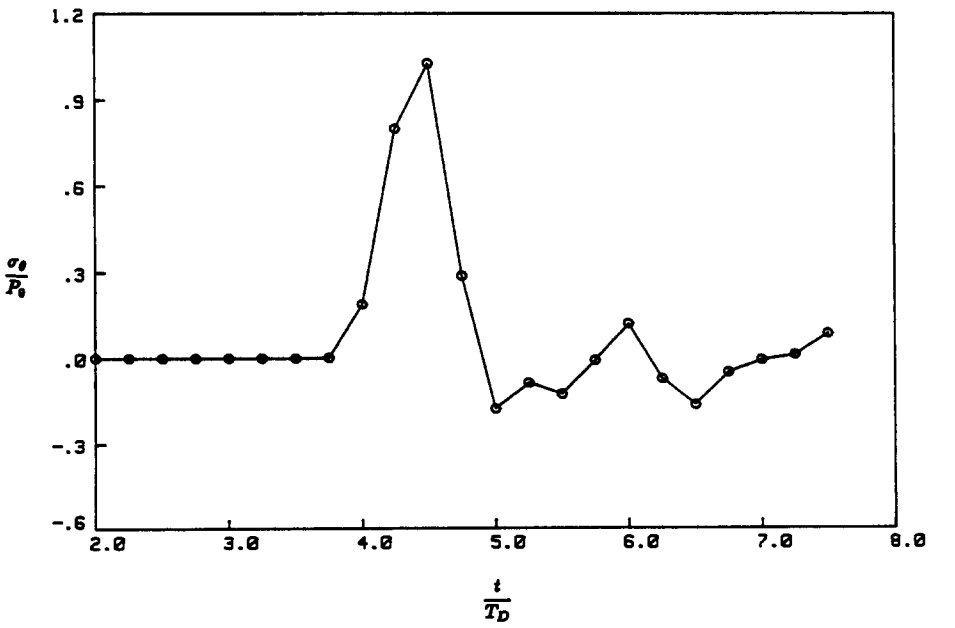

Fig. 17. Tangential stress at the top (point Q in Fig. 14) of the internal wall of an underground spherical shell.

CONCLUSION

The time domain axisymmetric transient elastodynamic analysis by BEM has been successfully implemented for the first time and also in a general system. The results are verified by showing comparisons between numerical results and the theoretical solutions. In the second example, the Rayleigh wave is generated by the present analysis although it is not implicitly or explicitly seen in the dynamic kernels. It has been clarified that the causality for BEM is still preserved for non-convex domain problems in the third example if the appropriate time steps and discretization are used. With the versatility of such a general system, it is possible to use sliding interfaces, spring supports, and higher order (cubic or quartic) interpolation functions. Some of these will be explored in a future publication by the authors.

REFERENCES

Ahmad, S. (1986). Linear and nonlinear dynamic analysis by boundary element method. Ph.D. Thesis, State University of New York at Buffalo.

Ahmad, S. and Banerjee, P. K. (1988). Time-domain transient elastodynamic analysis of 3-D solids by BEM. *Int. J. Num. Meth. Engng* **26**, 1709–1728.

Antes, H. and von Estorff, O. (1986) Dynamic soil–fluid interaction analysis by the boundary element method. In BETECH 86 (Edited by C. A. Brebbia and J. J. Corner), pp. 687–698. *Proc. 2nd Boundary Element Tech. Conf.*, M.I.T., Boston. CM Publ., Southampton.

Antes, H. and von Estorff, O. (1987). On causality in dynamic response analysis by time-dependent boundary element methods. *Earthquake Engng Struct. Dyn.* **15**, 865–870.

Banerjee, P. K. and Ahmad, S. (1985). Advanced three-dimensional dynamic analysis by boundary element. In *Proc. ASME Conf. on Advanced Topics in Boundary Element Analysis*, Florida, Nov. 1985, AMD, Vol. 72, pp. 65–81.

Banerjee, P. K., Ahmad, S. and Manolis, G. D. (1986). A time domain BEM for three-dimensional problems of transient elastodynamics. *Earthquake Engng Struct. Dyn.* **14**, 933–949.

Banerjee, P. K. and Butterfield, R. (1981). *Boundary Element Methods in Enginering Science*. McGraw-Hill, London.

Cole, D. M., Koslof, D. D. and Minster, J. B. (1978). A numerical boundary integral equation method for elastodynamics I. *Bull. Seism. Soc. Am.* **68**, 1331–1357.

Eringen, A. C. and Suhubi, E. S. (1975). *Elastodynamics*. Academic Press, New York.

Henry, D. P., Jr. and Banerjee, P. K. (1988). A variable stiffness type boundary element formulation for axisymmetric elastoplastic media. *Int. J. Num. Meth. Engng* **26**, 1005–1027.

Israil, A. S. M. and Banerjee, P. K. (1989). Advanced time-domain formulation of BEM for two-dimensional transient elastodynamics. To appear in *Int. J. Num. Meth. Engng*.

Karabalis, D. L. and Beskos, D. E. (1984). Dynamic response of 3-D foundations by time domain boundary element method. Final Report Part A, NSF Grant No. CEE-8024725, Department of Civil and Mineral Engineering, University of Minnesota, Minneapolis, Minnesota.

Mansur, W. J. and Brebbia, C. A. (1982). Numerical implementation of the boundary element method for two dimensional transient scalar wave propagation problems. *Appl. Math. Model.* **6**, 299–306.

Mansur, W. J. and Brebbia, C. A. (1985). Transient elastodynamics. In *Topics in Boundary Element Research* (Edited by C. A. Brebbia), Vol. 2, Chapter 5. Springer, Berlin.

Mayr, M., Drexler, W. and Kuhn G. (1980). A semianalytical boundary integral approach for axisymmetric elastic bodies with arbitrary boundary conditions. *Int. J. Solids Structures* **16**, 863–871.

Nigam, R. K. (1980). The boundary integral equation method for elastostatics problems involving axisymmetric geometry and arbitrary boundary conditions. M.S. Thesis, University of Kentucky.

Niwa, Y., Fukui, T., Kato, S. and Fujiki, K. (1980). An application of the integral equation method to two-dimensional elastodynamics. *Theo. Appl. Mech., J. Engng Fac. Tokyo University* **28**, 281–290.

Pekeris, C. L. (1955). The seismic surface pulse. *Proc. N.A.S.*, Vol. 41, pp. 469–480.

Rayleigh, Lord (1885). On waves propagated along the plane surface of an elastic solid. *London Math. Soc. Proc.*, Vol. 17, pp. 4–11.

Rice, J. M. and Sadd, M. H. (1984). Propagation and scattering of SH-waves in semi-infinite domain using a time-dependent boundary element method. *J. Appl. Mech. ASME* **51**, 641–645.

Rizzo, F. J. and Shippy, D. J. (1979) A boundary integral approach to potential and elasticity problems for axisymmetric bodies with arbitrary boundary conditions. *Mech. Res. Com.* **6**, 99–103.

Spyrakos, C. C. and Beskos, D. E. (1986). Dynamic response of rigid strip foundations by time domain boundary element method. *Int. J. Num. Meth. Engng* **23**, 1547–1565.

Timoshenko, S. P. and Goodier, J. N. (1979). *Theory of Elasticity*, 3rd Edn., pp. 510–513. McGraw-Hill, New York.

APPENDIX A: FUNDAMENTAL SOLUTIONS G_{ij}, F_{ij}

$$G_{ij}(x,t;\xi,\tau) = \frac{1}{4\pi\rho}\left\{(3a_{ij}-b_{ij})\int_{1/c_1}^{1/c_2}\lambda\delta(t-\tau-\lambda r)\,d\lambda + a_{ij}[\delta(t-\tau-r/c_1)\,c_1^2-\delta(t-\tau-r/c_2)/c_2^2]+b_{ij}\delta(t-\tau-r/c_2)/c_2^2\right\}$$

where

$$a_{ij} = \frac{y_i y_j}{r^3}, \quad b_{ij} = \frac{\delta_{ij}}{r}, \quad y_i = x_i - \xi_i.$$

$$\begin{aligned} F_{ij}(x,t;\xi,\tau) = \frac{1}{4\pi}\Big\{ & -6c_2^2(5a_{ij}-b_{ij})\int_{1/c_1}^{1/c_2}\lambda\delta(t-\tau-\lambda r)\,d\lambda \\ & +(12a_{ij}-2b_{ij})[\delta(t-\tau-r/c_2)-(c_2/c_1)^2\delta(t-\tau-r/c_1)] \\ & +2ra_{ij}c_2[\delta'(t-\tau-r/c_2)-(c_2/c_1)^3\delta'(t-\tau-r/c_1)] \\ & -c_{ij}(1-2c_2^2/c_1^2)[\delta(t-\tau-r/c_1)+(r/c_1)\delta'(t-\tau-r/c_1)] \\ & -d_{ij}[\delta(t-\tau-r/c_2)+(r/c_2)\delta'(t-\tau-r/c_2)]\Big\} \end{aligned}$$

where

$$a_{ij} = \frac{y_i y_j y_m n_m}{r^5}, \quad c_{ij} = \frac{y_j n_i}{r^3}, \quad d_{ij} = \frac{y_i n_j + \delta_{ij} y_m n_m}{r^3}, \quad b_{ij} = c_{ij} + d_{ij}.$$

APPENDIX B: CONVOLUTION INTEGRALS NEEDED FOR G_{ij} AND F_{ij}

$$\int_0^{\Delta t}\delta(t-\tau-r/c)\,d\tau = H(t-r/c)-H(t-\Delta t-r/c)$$

$$\int_0^{\Delta t}\tau\delta(t-\tau-r/c)\,d\tau = (t-r/c)[H(t-r/c)-H(t-\Delta t-r/c)]$$

$$\int_0^{\Delta t}\int_{1/c_1}^{1/c_2}\lambda\delta(t-\tau-\lambda r)\,d\lambda\,d\tau = \{\lambda^2/2[H(t-\lambda r)-H(t-\Delta t-\lambda r)]\}_{1/c_1}^{1/c_2}$$

$$\int_0^{\Delta t}\int_{1/c_1}^{1/c_2}\lambda\tau\delta(t-\tau-\lambda r)\,d\lambda\,d\tau = t\{\lambda^2/2[H(t-\lambda r)-H(t-\Delta t-\lambda r)]\}_{1/c_1}^{1/c_2} - \{\lambda^3\,3[H(t-\lambda r)-H(t-\Delta t-\lambda r)]\}_{1/c_1}^{1/c_2}$$

$$\int_{(n-1)\Delta t}^{n\Delta t}\delta(t-\tau-r/c)f(x,\tau)\,d\tau \cong \frac{f(x,n\Delta t)-f(x,(n-1)\Delta t)}{\Delta t}[H(t-(n-1)\Delta t-r/c)-H(t-n\Delta t-r/c)].$$